

# Generative detect for occlusion object based on occlusion generation and feature completing

Can Xu<sup>1</sup>, Peter Yuen<sup>3</sup>, Wenxi Lang<sup>4</sup>, Rui Xin<sup>5</sup>, Kaichen Mao<sup>1</sup>, Haiyan Jiang<sup>1,2\*</sup>

1 College of Artificial Intelligence, Nanjing Agricultural University, Nanjing,  
210095, Jiangsu, China

2 National Engineering & Technology Center for Information Agricultural,  
Nanjing Agricultural University, Nanjing, 210095, Jiangsu, China

3 Electro-Optics & Remote Sensing, Centre for Electronics Warfare, Information &  
Cyber (CEWIC), Cranfield University, Swindon, U.K

4. College of Computer Science and Technology, Nanjing University of Aeronautics  
and Astronautics, Nanjing, 211106, Jiangsu, China

5. Department of Computer Science, Durham University, UK

**Abstract:** Detecting the object with external occlusion has always been a hot topic in computer vision, while its accuracy is always limited due to the loss of original object information and increase of new occlusion noise. In this paper, we propose a occluded object detection algorithm named GC-FRCN (Generative feature completing Faster RCNN), which consists of the OSGM (Occlusion Sample Generation Module) and OSIM (Occlusion Sample Inpainting Module). Specifically, the OSGM mines and discards the feature points with high category response on the feature map to enhance the richness of occlusion scenes in the training data set. OSIM learns an implicit mapping relationship from occluded feature map to real feature map adversarially, which aims at improving feature quality by repair the noisy object feature. Extensive

24 experiments and ablation studies have been conducted on four different datasets. All  
25 the experiments demonstrate the GC-FRCN can effectively detect objects with local  
26 external occlusion and has good robustness for occlusion at different scales.

27 **Keywords:** Occlusion; Object detection; Feature completing; Generative Adversarial  
28 Networks;

## 29 1 Introduction

30 Object detection has always been an active field in computer vision research. Its  
31 goal is to learn a visual model for several kinds of objects and then use the model to  
32 predict the category and position of objects in the image. In recent years, thanks to the  
33 development of the convolutional neural network, related researches (Ren et al., 2016;  
34 Cai et al., 2016; He et al., 2017; Law et al., 2018; Lu et al., 2018; Zhou et al., 2019;  
35 Duan et al., 2019) on object detection have made a tremendous breakthrough in  
36 detection accuracy and speed, but the detection accuracy of objects which are in some  
37 complex scenes still needs to be further improved. The complexity is usually  
38 manifested by the presence of disturbing objects in the scene that are unrelated to the  
39 object to be detected. A typical example is that the detector may confuse trees with  
40 pedestrians at certain moments in the automatic drive. However, compared with the  
41 distinction between trees and pedestrians, the more difficult scene is to detect  
42 pedestrians blocked by trees, that is, to achieve accurate detection of blocked objects.  
43 For occluded objects, the loss of original object information and the mixing of  
44 irrelevant information increases the difficulty of feature learning. The low feature  
45 quality makes the detection results often contain a large number of False Negative

46 samples. Therefore, how to realize the effective detection of the occluded objects has  
47 become the most important challenge of the detection algorithm in practical  
48 application.

49 Occlusion is a complex problem of optics and geometry. According to the causes,  
50 occlusion can be divided into two categories: intra-class occlusion and inter-class  
51 occlusion (Wang et al., 2018). In-class occlusion appears when the objects to be  
52 detected blocked by other objects in the same category, and studies have shown that  
53 (Ouyang et al., 2013; Tian et al., 2015) it mainly affects the positioning accuracy. That  
54 is, the detector can easily move the prediction box of object A to object B, which  
55 overlaps with object A. In recent work, Wang (Wang et al., 2018) designed a new  
56 constraint named Repulsion loss to promote each prediction box close to its ground  
57 truth box, while away from the ground truth box of other objects as far as possible.  
58 Zhang proposed a new detection algorithm named Occlusion Aware R-CNN, which  
59 designed the aggregation loss and PORoI to train several local detectors for the  
60 sub-area of the occluded object. By calculating the category probability and prediction  
61 frame coordinates, it finally fuses the results of every local detector, which improved  
62 the detection accuracy of the crowded pedestrians with the intra-class occlusion.

63 Here, we keep the point on the inter-class occlusion. Inter-class occlusion refers  
64 to the external occlusion caused by the coverage of different kinds of objects, whose  
65 difficulty lies in the poor feature representation of objects when detecting. Compared  
66 with conventional objects, it is harder to obtain high-quality features of inter-class  
67 occluded objects. Firstly, occlusion from other objects results in the loss of significant

68 information of the object to be detected. On this basis, the features learnt cannot fully  
69 represent the object even if using the convolution neural network. Besides, occlusion  
70 means the original object data space will be mixed with noise. Furthermore, these  
71 local noises can be gradually transferred to the global feature with high-semantic  
72 information in the process of feature learning. Therefore, for the inter-class occlusion  
73 objects, how to achieve high-quality representation of object features is the key to  
74 improve the detection accuracy.

75 Different from Bell (Bell et al., 2016) and Lin (Lin et al., 2017) who fuse multiple  
76 convolution features to improve the feature quality of conventional objects, existing  
77 studies on occlusion detection (Pepik et al., 2013; Mathias et al., 2013; Tang et al.,  
78 2014; Gidaris et al., 2015; Zhou et al., 2017; Noh et al., 2018) pay more attention to  
79 mining the visible part. The core solution is: learning a series of local detectors for  
80 each part of the blocking object and using a specific strategy to fuse the results of  
81 local detectors to infer the final detection results of the whole object. Recently, Zhou  
82 (Zhou et al., 2017) proposed an occlusion detection method based on analyzing local  
83 occlusion and multi-label learning. By combining multiple local detectors, the  
84 correlation between local detectors is enhanced, which reduces the calculation cost  
85 and improves the detection accuracy of shielded objects. Noh (Noh et al., 2018)  
86 calculated the confidence of different regions of the occluded object and used the  
87 detection results of these visible regions to correct the final detection results of the  
88 whole object. Further analysis, we find that while exert visible region information  
89 fully may be effective to reduce the block noise, but to some extent also split the

90 structure information between different parts, which caused a massive change on the  
91 results when combining different local regions to test. So, in this case, some specific  
92 prior knowledge of the occluded object is needed when designing the local detectors,  
93 which limit the generalization ability.

94 When it comes to improving the feature quality of the occluded object, the  
95 existing researches entirely mine the visible information of the unshaded area to  
96 suppress the occluded noise. Our solution is to complete the occlusion noise in the  
97 global feature map as we regard the inter-class occluded objects as the superposition  
98 of occlusion noise and original object information. We design a detection algorithm  
99 named GC-FRCN by introducing generative adversarial network to the Faster-RCNN  
100 [Ren et al., 2015], which mainly includes the OSGM and OSIM. The OSGM can  
101 simulate occlusion scenes by discarding the feature points with high category  
102 response on the feature map, aiming to construct training data that covers as many  
103 occlusion scenarios as possible to improve model's occlusion detection capability. The  
104 OSIM learns the implicit mapping relationship from occluded feature to real feature,  
105 and finally remove occlusion noise from the object's feature map. To ensure the  
106 mapping effectiveness, we make most use of the richer image information and  
107 constrain the mapping relation by keep the occluded images as similar as the real  
108 scene in both local details and global structure. The main contributions of this paper  
109 are as follows:

110 (1) We address the occluded object detection problem by expanding the richness of  
111 the occlusion scene and cleaning occlusion noise, and propose a cascading occlusion

112 detection algorithm GC-FRCN consisting of occlusion generation module OSGM and  
113 feature repair module OSIM. Experimental results on four different data sets  
114 demonstrate its superior performance.

115 (2) Different from the existing work, the simple yet effective OSGM discards the  
116 feature point with high category response and simulates different occluded scenes  
117 based on the analysis of effective receptive field. Our results show this strategy  
118 benefits the occlusion detection capability.

119 (3) With the implicit mapping relationship learnt by adversarially minimizing the  
120 difference between the occluded images and real scene in both local details and global  
121 structure, the OSIM can remove occlusion noise from the object's feature map. Our  
122 results show the OSIM has good robustness for occlusion at different scales.

## 123 2 Related work

### 124 2.1 Generic Object Detection

125 Early researches on object detection relied on artificial features and classifiers to  
126 searching for the object to be detected in the image (Papageorgiou et al., 2000; Viola  
127 et al., 2004; Felzenszwalb et al., 2008; Felzenszwalb et al., 2009; Dollar et al., 2014).  
128 However, the detection accuracy is always unable to meet the actual application  
129 requirements, for the artificial features cannot express the object effectively. In recent  
130 years, due to the rapid development of convolution neural network, object detection  
131 algorithms based on deep learning have achieved breakthroughs in both detection  
132 accuracy and speed, which are mainly divided into two types: two-stage and  
133 single-stage object detection methods. Different from searching for regions of interest

134 violently, the two-stage detection algorithm uses the generative strategy to produce  
135 proposals, which mainly includes RCNN (Girshick et al., 2014) and its subsequent  
136 improvements. RCNN automatically generates a set of candidate regions based on  
137 Selective Search algorithm (Uijlings et al., 2013), and then uses SVM and linear  
138 regression to achieve classification and position box fine-tuning, respectively. For its  
139 problem of extracting proposals' features repeatedly which cost a large of training  
140 resources, He (He et al., 2015) proposed a detection method based on spatial pyramid  
141 pooling which gets the proposals' features by mapping candidate regions on the global  
142 feature map; while Girshick (Girshick et al., 2015) directly trained an "end-to-end"  
143 CNN network to reduce the training volume. Furthermore, Faster RCNN (Ren et al.,  
144 2015) and R-FCN (Dai et al., 2016) combined the generation of candidate regions and  
145 detection of proposals into a whole network, which fine-tunes the entire network  
146 during training without storing a large number of features. Compared with the  
147 two-stage detection methods, the single-stage detection methods (Redmon et al., 2016;  
148 Liu et al., 2016; Redmon et al., 2017; Redmon et al., 2018) take the input image as a  
149 candidate region, and return object's boundary box coordinates and category on the  
150 preset anchor frames, which further improve the training efficiency and detection  
151 speed of the detector.

## 152 2.2 Data Augmentation

153 Sufficient training data is the foundation for constructing a deep learning model.

154 The CNN gradually abstracts the features from the original images, so the quality and

155 quantity of training images have a direct effect on features' effectiveness. As a result,

156 the performance of the detector will generally improve with the increase of the scenes  
157 containing objects in training data. However, collecting and making an extensive  
158 detection data set is so difficult that the usual treatment is to expand and enhance the  
159 available training data through operations such as rollover, rotation, scaling, clipping  
160 and shifting. Meanwhile, some studies (Simo et al., 2014; Loshchilov et al., 2015;  
161 Wang et al., 2015) also explored how to fully mine and utilize the limited training data  
162 to improve the accuracy and robustness of the detector. Shrivastava (Shrivastava et al.,  
163 2016) proposed a detection method based on difficult sample mining, which  
164 significantly improved the detection accuracy by retraining samples with massive  
165 losses. Wang (Wang et al., 2017) also showed that the detector's robustness on  
166 shielding and deformation could be improved by continuously constructing shielding  
167 and deformation samples when training the detector. In this paper, we are also  
168 inspired by data enhancement to generate a large number of occlusion samples to  
169 enhance the diversity of training data and further improve the detection performance  
170 of the model for inter-class occlusion objects.

### 171 2.3 Feature Completing

172 For inter-class occluded objects, we hope to restore noise in the features as the  
173 real information partially lost due to occlusion, to improve the feature quality as well  
174 as detection accuracy. Although the research of feature repairing is still in the initial  
175 stage, the problem of image repairing has been widely studied. The purpose of image  
176 repairing is to automatically recover the lost content in the image, whose early  
177 methods focus on repairing by spreading the known local information to the unknown.



178 With the breakthrough of the generative adversarial network in the application of  
179 image repairing, relevant researches (Xiang et al., 2017; Lahiri et al., 2017; Yeh et al.,  
180 2017; Dolhansky et al., 2018) have achieved more accurate results not only in  
181 semantic but also the visual effect of repairing details. Recent studies expand the  
182 structure of the generative adversarial network by using multiple discriminators to  
183 improve the repairing effect further. Pathak (Pathak et al., 2016) proposed an  
184 encode-decode network for image repairing; and then Iizuka (Iizuka et al., 2017)  
185 designed the repair network based on local and global discrimination models, which  
186 realized the optimization of local details and overall texture of the image. On this  
187 basis, Li (Li et al., 2017) further added the semantic parsing model to optimize the  
188 face structure information, which reduces the error to the human eye level. Yu (Yu et  
189 al., 2018) abstracted the repair process into two encode-decode steps and further  
190 optimized the repair results with coarse precision by using counter loss, which  
191 significantly improved the repair accuracy.

### 192 3 Generative Features Completing

193 Based on the data-driven strategy, we improved the feature quality and  
194 constructed the occlusion object detector by expanding the richness of the occlusion  
195 scene and cleaning occlusion noise in the feature. Here, the key is how to generate  
196 representative occlusion data and repair occlusion noise, for which we designed  
197 OSGM and OSIM, respectively.

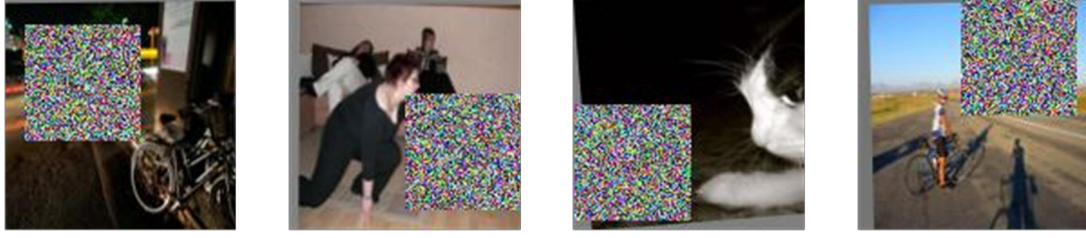
## 198 3.1 OSGM: Refinement for the Occlusion Generation

### 199 3.1.1 Analysis of Occlusion Simulation

200 Deep learning methods are always based on large-scale data learning to achieve  
201 the abstraction and modelling of a certain type of problem. When detecting objects  
202 with local occlusion, the simple solution is to construct a data set covering all  
203 occlusion scenarios. However, collecting a sufficiently large occluded data set is  
204 complicated and low cost-effective. Without extra data collection work, a feasible  
205 occlusion simulation method is to randomly discard pixels of different combinations  
206 on the existing detection data set. However, it cannot guarantee the effectiveness and  
207 representativeness of occlusion scenes. As shown in Fig. 1, objects are not blocked in  
208 some images because positions of objects to be detected and the pixels to be discarded  
209 are random. With the decrease of the discarded size, the number of similar invalid  
210 samples will further increase substantially. For the same object, there will be much  
211 redundancy when simulating different occlusion scenes, whose occlusion expression  
212 may be more similar after feature learning. Invalid samples and repeated samples do  
213 not help improve the performance of the model but bring additional computational  
214 overhead for feature learning and subsequent repair.



a) Repeated occlusion scenarios



b) Invalid occlusion scenarios

Fig. 1 Examples of invalid and repeated occlusion scenarios

### 215 3.1.2 Design of Occlusion Simulation

216 Based on the analysis in section 3.1.1, we hope that occluded image generated not  
 217 only represent a kind of occlusion scene, but also the object is always blocked. For  
 218 this reason, we firstly discard pixels on the feature map to ensure enough differences  
 219 of different occlusion scenes generated based on the same object. During feature  
 220 learning, the original input image will be abstracted into the feature map iteratively,  
 221 and the pixels on the feature map have more robust semantics than the original image.  
 222 Different feature maps after discarding pixels can be approximated as the abstraction  
 223 of different occlusion scenes. The area of the image that any pixel of the feature map  
 224 corresponding to can be described as a theoretical receptive field. When generating  
 225 occluded samples, what we need to drop out is these pixels in the theoretical receptive  
 226 field of the input image. For a specific network, the calculation method of the  
 227 theoretical receptive field is shown in formula (1).

$$228 \quad S_{RF}(t) = (S_{RF}(t-1) - 1)N_s(t) + S_f(t) \quad (1)$$

229 Where the  $S_{RF}(t)$  means the theoretical field size of convolution layer  $t$ , while  
 230  $N_s(t)$  and  $S_f(t)$  is the stride and convolution kernel size of convolution layer  $t$ .

231 In order to eliminate invalid occlusion scenes, we also want to discard pixels that  
 232 are highly relevant to the object. Luo (Luo et al., 2016) found that although the value

233 of pixel on the feature map is determined by the value in the receptive field of image,  
 234 the correlation degree between different image pixels and feature map pixels is quite  
 235 different. Compared with the pixels at the edge of the image, the pixels in the middle  
 236 of the image have more influence on the value of feature map, and the effective  
 237 receptive field which actually decides the value of feature map is always smaller than  
 238 the theoretical receptive field. In other words, compared with the edge, the pixels in  
 239 the middle of feature map are affected by more original image information during the  
 240 convolution calculation, which means a higher probability to contain the original  
 241 information of the object. We chose to discard the pixels in the middle of the feature  
 242 map which are more relevant to the target to be detected. For the  $N \times N$  feature map,  
 243 if the pixel coordinates of its upper left vertex are denoted as  $(x_0, y_0)$ , the range of  
 244 disposable pixel coordinates  $(X_{erf}, Y_{erf})$  can be calculated by formula (2)-(4).

$$245 \quad \begin{aligned} X_{erf} &\in (x_0 + [\alpha * N], x_0 + [(1 - \alpha) * N]) \\ Y_{erf} &\in (y_0 + [\beta * N], y_0 + [(1 - \beta) * N]) \end{aligned} \quad (2)$$

$$246 \quad \alpha = \frac{w_{obj}}{w_{in}} \quad (3)$$

$$247 \quad \beta = \frac{h_{obj}}{h_{in}} \quad (4)$$

248 Where  $\alpha$  and  $\beta$  represents the significant discard coefficient;  $w_{obj}$  and  $h_{obj}$   
 249 represents the width and length of the object's minimum enclosing rectangle;  $w_{in}$   
 250 and  $h_{in}$  means the width and length of the input image, respectively.

### 251 3.1.3 Structure of OSGM

252 As shown in Fig. 2, the basic structure of OSGM is from the conv1 layer to the  
 253 pool3 layer of VGG16 network. For all the convolution layers, we adopt the kernel of  
 254  $3 \times 3$  and add standard Batch-Normalization and Relu operation. While for the

255 pooling layers, we use max pooling with a kernel of  $2 \times 2$ . OSGM determines the  
 256 pixels' effective discard range of feature map using the formula (2) - (4) and  
 257 calculates the receptive field using the formula (1). Then, we set the values of all  
 258 pixels as 0 in the corresponding to the receptive field, which is mapped by the pixel  
 259 drop out from the feature map. Here, we directly reuse the VGG16 model trained on  
 260 the ImageNet data set to initialize the parameters of OSGM. Besides, in order to  
 261 further enhance the richness and difficulty of occluded samples, we designed four  
 262 different occlusion templates with the size of  $1 \times 1$ ,  $1 \times 2$ ,  $2 \times 1$  and  $2 \times 2$  when  
 263 discarding pixel points in the feature map.

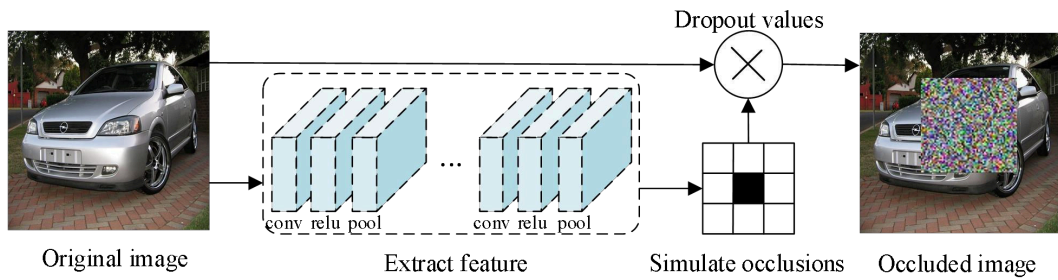


Fig. 2 Structure and workflow of the OSGM module

## 264 3.2 OSIM: Refinement for the Occlusion Representation

### 265 3.2.1 Overview of Occlusion Inpainting

266 For the object with local occlusion, the occlusion noise mixed with the original  
 267 data space will run through the feature learning, resulting an upper limit of detection  
 268 accuracy. Our innovative idea is to learn an implicit mapping relationship from  
 269 occluded feature map to real feature map. To realize this goal, as shown in Fig. 3,  
 270 OSIM is composed of one Generator and two discriminators, which make the repaired  
 271 region consistent with the real label both in local details and overall structure.

272 3.2.2 Generator

273 The generator is described as a process of feature learning and generating new  
 274 feature values for the occlusion region. As shown in Fig. 3, after the generator  
 275 learning the object features based on the encoding, it generates new feature values for  
 276 the occlusion object and then passes them to the discriminator. The encoding network  
 277 is based on the conv1 to pool2 layers of the VGG16 network (Simonyan et al., 2014),  
 278 where the convolution kernel is  $3 \times 3$  and the max pooling kernel is  $2 \times 2$ . We use  $L_2$   
 279 loss to measure the difference between generated features and real features. The  $L_2$   
 280 loss function of the generator is shown in formula (5).

281 
$$L_G = \frac{1}{2M} \sum_{i=1}^M \|x_i - x'_i\|_2^2 \quad (5)$$

282 Where  $M$  is the number of pixels on the feature map,  $x_i$  and  $x'_i$  means the real and  
 283 the generated feature pixels.

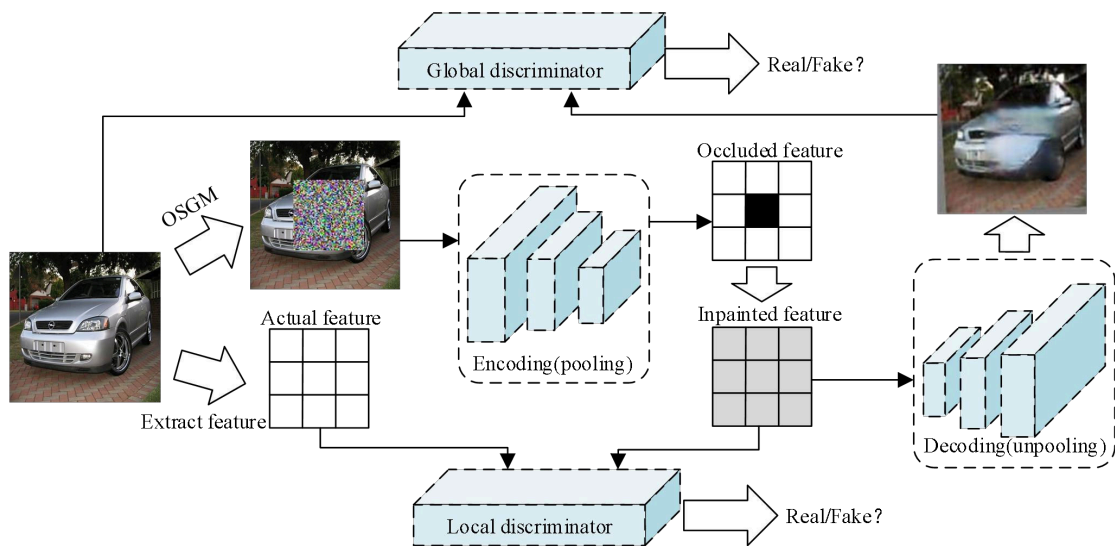


Fig. 3 Structure and workflow of OSIM module

284 3.2.3 Discriminator

285 The generator makes a narrow gap between the feature values containing block  
 286 noise and its corresponding real values, but it cannot guarantee the repaired features

287 similar to the real features in terms of content and distribution. It is because the  $L_2$   
 288 loss punishes the outliers seriously and does not consider the local context  
 289 information and structural relationship between the occluded region and its adjacent  
 290 region. Ideally, the restored features should be not only similar to the real features in  
 291 content, but also be similar to the surrounding regions in structure. For this reason, we  
 292 designed the local discriminator and global discriminator, respectively in OSIM to  
 293 constraint the features generated further. As shown in Fig. 3, the local discriminator  
 294 focuses the attention of the generator on the internal details of the occlusion region,  
 295 which helps the repaired features to be consistent with the real features in terms of  
 296 pixel value and statistical distribution. The global discriminator maps the restored  
 297 features to the same size as the input image through the decoding network, which  
 298 normalizes the structural relationship by identifying the similarity between the  
 299 original input image and the image upsampled from the repaired feature map. It  
 300 should be noted that, the structure of the encoding network and the decoding network  
 301 is symmetrical, while the only difference between the two networks is that the  
 302 un-pooling layer is used to replace the pooling layer in the decoding network.

303 We also note that the network structure of the local discriminator and the global  
 304 discriminator is similar to the research proposed by Radford (Radford et al., 2016).  
 305 Furthermore, the two discriminators also have the same loss function which is shown  
 306 in formula (6).

$$L_{localD} = L_{globalD} = \min_G \max_D E_{x \sim P_{data}(x)} [\log D(x)] + E_{z \sim P_z(z)} [\log (1 - D(G(z)))] \quad (6)$$

307

308 Where  $L_{localD}$  and  $L_{globalD}$  represents the loss function of local discriminator and  
309 global discriminator,  $E_{y \sim P_{data}(y)}$  and  $E_{z \sim P_z(z)}$  represents the distribution of the true  
310 image pixels and occluded noise. The loss function  $L$  of OSIM module consists of  
311 generator and discriminator which can be calculated by formula (7).

$$312 \quad L = L_G + \gamma_1 L_{localD} + \gamma_2 L_{globalD} \quad (7)$$

313 Where  $\gamma_1$  and  $\gamma_2$  are used to balance the loss of different parts, and the  
314 default value is both 300.

## 315 4 GC-FRCN: Approach Details

### 316 4.1 Structure of GC-FRCN

317 As shown in Fig. 4, GC-FRCN takes Faster-RCNN as the basic network structure,  
318 and includes five key steps: occluded data generation based on OSGM, feature  
319 learning, repairing feature based on OSIM, candidate region generation, object  
320 classification and position box regression. To ensure the reuse of occluded data set  
321 generated, OSGM is designed as an independent module which cascade integrated  
322 into GC-FRCN. For the different occluded data generated by OSGM, GC-FRCN uses  
323 the convolution neural network to learn the global features of the whole image and  
324 outputs the feature map. Here, the critical role of OSIM is to provide more accurate  
325 feature representation of blocked objects, so the OSIM is embedded as a plug-in after  
326 the feature learning step which is trained independently and transmits the repaired  
327 feature map to the RPN (Region proposal network, RPN). RPN uses the sliding  
328 window to traverse the repaired feature map, and sets 9 rectangular regions (3 aspect  
329 ratios  $\times$  3 scales) to generate candidate regions when mapping each pixel of the



330 feature map. Finally, the restored features are maximally pooled to obtain the features  
 331 of each candidate regions, which are fed into a cascade of entirely complex networks  
 332 to achieve the final category and position box.

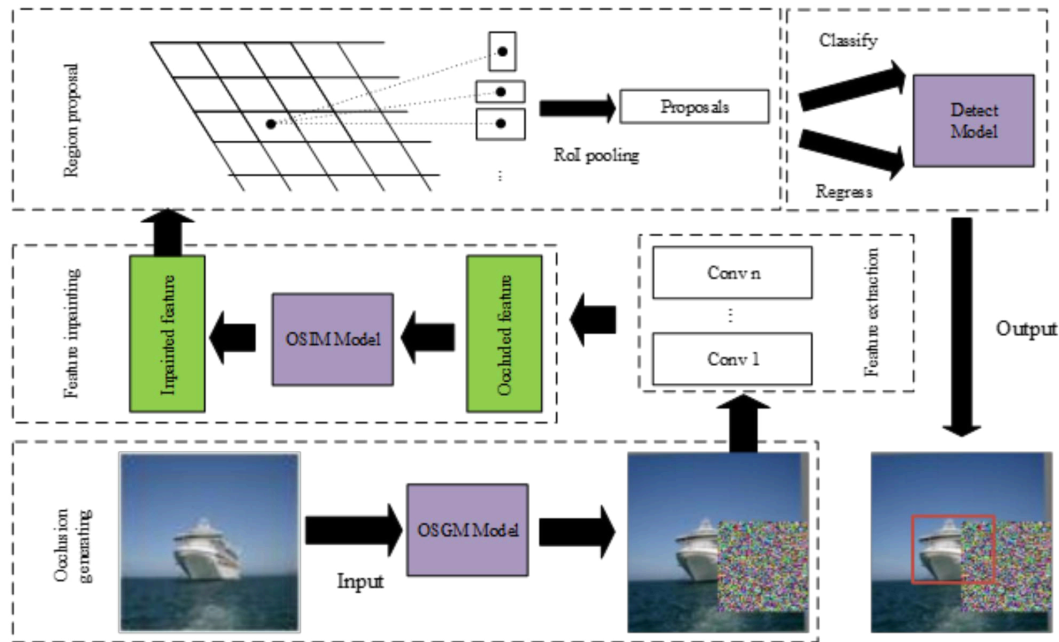


Fig. 4 Structure and workflow of GC-FRCN module

#### 333 4.2 Independent Training for GC-FRCN

334 In this study, the training of GC-FRCN includes two parts: training the OSIM and  
 335 training the detector. When training the repair model OSIM, the generation loss  $L_G$  is  
 336 used firstly to fill the initial eigenvalue for the occluded object; and then the  
 337 discriminator loss  $L_D$  is used to improve the precision of the eigenvalue. We  
 338 initialize the parameters of OSIM randomly at the beginning of training, but the  
 339 model of the latter stage is trained based on the model obtained from the previous  
 340 stage in order to improve the training efficiency and model accuracy. When training  
 341 the detector, we follow the setup of standard Faster RCNN based on SGD (Stochastic  
 342 gradient descent, SGD) and alternate optimization strategy, where the only difference  
 343 is the feature passed to RPN optimized by the repair model in the first place. The loss

344 function of the detector is composed of classification loss and regression loss, which  
 345 are normalized by  $N_{cls}$  and  $N_{reg}$  and then weighted by equilibrium parameters  $\lambda$  ().  
 346 The loss function is shown in formula (8).

$$347 \quad L(\{P_i\}, \{t_i\}) = \frac{1}{N_{cls}} \sum_i L_{cls}(P_i, P_i^*) + \lambda \frac{1}{N_{reg}} \sum_i P_i^* L_{reg}(t_i, t_i^*) \quad (8)$$

348 Here,  $N_{cls}$  represents the mini-batch size of training,  $N_{reg}$  represents the number of  
 349 candidate regions and the  $i$  is the anchor number.  $P_i$  is the probability of the anchor  
 350 point being as an object, and the corresponding  $P_i^*$  value is given as 1 when the  
 351 anchor point is predicted as positive and otherwise it is 0 if the anchor is negative.  $t_i$   
 352 and  $t_i^*$  represent the coordinates of the upper left and lower right vertex of the  
 353 predicted bounding box respectively. The  $L_{cls}$  and  $L_{reg}$  can be calculated by  
 354 formula (9) and (10).

$$355 \quad L_{cls}(P_i, P_i^*) = -\log [P_i^* P_i + (1 - P_i^*)(1 - P_i)] \quad (9)$$

$$356 \quad L_{reg}(t_i, t_i^*) = \begin{cases} 0.5(t_i - t_i^*)^2 & |t_i - t_i^*| < 1 \\ |t_i - t_i^*| - 0.5 & |t_i - t_i^*| \geq 1 \end{cases} \quad (10)$$

## 357 5 Experiment

### 358 5.1 Datasets and Evaluation Metrics

359 To verify the performance of GC-RFCN, we had carried out several experiments  
 360 on four data sets of PASCAL VOC 2007, VOC 2012 (Everingham et al., 2010), MS  
 361 COCO (Lin et al., 2014) and PANICLE2017. The PANICLE2017 is an image data set  
 362 containing rice panicles covered by leaves. As shown in Fig. 5, PANICLE2017  
 363 consists of two parts. The first one is marked according to the format of VOC, which  
 364 is used to train the rice panicle detector. The training data set, verification set and test  
 365 set are composed of 2080, 912 and 1280 field rice images, respectively. The other part

366 is composed of 982 images of unshaded rice panicles, which are used to train the  
 367 occlusion feature repair model.

368 We conducted most of the ablation studies on the PASCAL VOC 2007 data set  
 369 and the COCO data set and reported the results of verification of the actual  
 370 application effect on the PANICLE2017 data set. First, we select the mean average  
 371 precision (mAP) and mean average recall (mAR) to evaluate the performance of  
 372 GC-FRCN on VOC and COCO data sets, as shown in formula (11) and (12).

$$373 \quad \text{mAP} = \frac{1}{m} \sum_{i=1}^n P_i (R_i - R_{i-1}) \quad (11)$$

$$374 \quad \text{mAR} = \frac{1}{m} \sum_{i=1}^n 2 \int_{0.5}^1 R_{IoU} d(IoU) \quad (12)$$

375 Where  $R_i$  represents the different recalls ranked according to the confidence degree,  
 376 and  $P_i$  represents the maximum precision corresponding to the  $R_i$ . And the  $R_{IoU}$   
 377 means the recall corresponding to the IoU (Intersection-over-Union, IoU). Secondly,  
 378 in order to estimate the restoration accuracy of OSIM quantitatively, SSIM (structural  
 379 similarity index) was selected to evaluate the difference of images before and after  
 380 image restoration, which can be calculated in formula (13).

$$381 \quad \text{SSIM}(x, y) = \frac{(2\mu_x\mu_y+c_1)(\sigma_{xy}+c_2)}{(\mu_x^2+\mu_y^2+c_1)(\sigma_x^2+\sigma_y^2+c_2)} \quad (13)$$

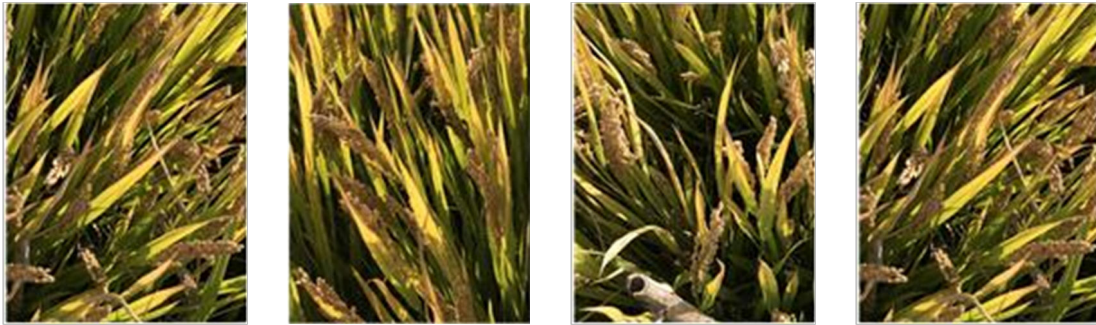
382 Where  $x$  and  $y$  represents the original image and recovered image;  $\mu$  and  $\sigma$   
 383 represents the average and the standard deviation of  $x$  and  $y$ , while the  $\sigma_{xy}$  means  
 384 the covariance of  $x$  and  $y$ ; The  $c_1$  and  $c_2$  are constants to avoid the denominator  
 385 being 0 whose default value are 6.5025 and 58.5225, respectively. Thirdly, we select  
 386 the counting accuracy and the classification accuracy to evaluate the performance of  
 387 GC-FRCN on PANICLE2017 data set. The counting accuracy  $P_c$  refers to the ratio

388 of detecting the correct number of panicles to the actual number of panicles; while the  
 389 classification accuracy  $P_t$  is the correct number of panicles identified as panicles  
 390 (true positive) to the number of all objects identified as panicles (true positive and  
 391 false positive) in the imagery data set:

$$392 \quad P_c = \frac{N_{cor}}{N_{real}} \times 100\% \quad (13)$$

$$393 \quad P_t = 1 - \frac{N_{err}}{N_{dect}} \times 100\% \quad (14)$$

394 Where  $N_{cor}$  and  $N_{err}$  are the correct (true positive) and wrong (false positive)  
 395 number of panicles detected by the model, respectively;  $N_{real}$  and  $N_{dect}$  represents  
 396 the actual number of panicles and all the objects identified as panicles in the test  
 397 sample.



(a) Training images of VOC2017 dataset for the detect model



(b) Training images of PANICLE2017 dataset for the detect model

Fig. 5 Training images of PANICLE2017 rice data set

## 398 5.2 Experiment Settings

399 As described in section 3.1, all experiments were simulated by OSGM module to  
 400 reconstruct the experimental data set. For VOC data sets, we used ‘trainval’ set and

401 ‘test’ set for training and testing, respectively. For the feature repair model, we used a  
402 250K SGD training generator and discriminator by keeping the learning rates at  
403 0.0001 and 0.0002, respectively. For the detector, the number of iterations is 80 k and  
404 the learning rate starts from 0.001 and decreases to 0.0001 after 60K iterations. Also,  
405 we followed most of the training setups of the standard Faster RCNN (Ren et al.,  
406 2015) with a mini batch size of 2 images and candidate regions of 256. For the COCO  
407 data set, we used ‘trainval35k’ set and ‘minival’ set for training and testing,  
408 respectively. The parameters of feature repair model are the same as those of VOC  
409 data set. For the detector, the number of iterations is 320K, and the initial learning rate  
410 is 0.001, which decreases to 0.0001 after 280K iterations. For the PANICLE2017 data  
411 set, the feature repair model and detector will keep all parameter settings consistent  
412 with the VOC data set.

413 When test the model, the experimental results of PANICLE2017 data set were  
414 obtained from the test set composed of real field scenes. For the VOC data set and the  
415 COCO data set, we generate occlusion at different scales (small, medium and large)  
416 on the ‘test’ set of VOC and ‘minival’ set of COCO using four discard the template  
417 ( $1 \times 1$ ,  $1 \times 2$ ,  $2 \times 1$  and  $2 \times 2$ ). Especially, the small, medium and large scale mean the  
418 about 6%, 14% and 25% pixel loss of the whole image respectively, while means the  
419 14%~22%, 20%~31% and 46%~60% pixel loss of the object to be detected.

## 420 5.3 Results on PASCAL VOC 2007

### 421 5.3.1 Quantitative Evaluations of GC-FRCN

422 In order to verify the effectiveness of GC-FRCN, we select the classical Faster

423 RCNN as the baseline and combine our OSGM and OSIM to train detectors,  
 424 respectively. The results are shown in Table 1. Taking small scale occlusion and ZF  
 425 network as an example, mAP of baseline is 48.6%, which has an increase of 2.8% and  
 426 3.3% after adding OSGM module and OSIM respectively. While the static  
 427 Faster-RCNN with ZF-net achieves a mAP of 58.7% on the VOC 2007 test without  
 428 occlusion, which is about 32% and 10% higher than the big occlusion and small  
 429 occlusion. From this point of view, we can find the occlusion has a significant effect  
 430 on the detect results, and the difficulty of repairing the detecting is increasing with the  
 431 size of occlusions. All these rising trends are also reflected in the test results of large  
 432 and medium scale occlusion.

433 Table 1 Mean average precision for **VOC 2007 test** with different size of occlusions

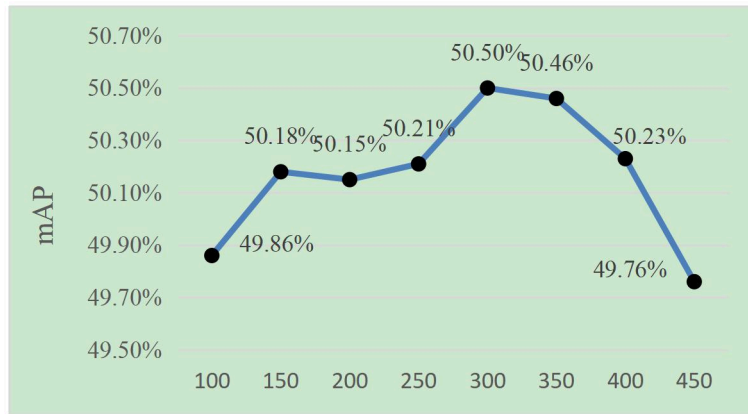
Method	Arch	Mechanism		mAP of different occlusion(%)			
		+OSGM	+OSIM	Big	Middle	Small	None
Faster-RCNN(Baseline)	VGG16			36.9%	53.5%	59.3%	66.9%
	VGG16	✓		43.9%	55.1%	61.5%	/
	VGG16		✓	48.1%	59.4%	63.5%	/
	ZF			26.7%	41.7%	48.6%	58.7%
	ZF	✓		33.9%	41.1%	51.4%	/
	ZF		✓	38.9%	48.6%	52.9%	/
A-FRCN	VGG16			45.2%	53.7%	60.6%	69.1%
YOLO	VGG16			43.6%	52.7%	58.8%	65.8%
YOLO V3	VGG16			47.3%	58.6%	63.6%	76.3%
SSD	VGG16			46.4%	58.1%	62.9%	72.2%
GC-FRCN (Ours)	VGG16	✓	✓	50.5%	61.1%	65.1%	69.9%

434 We compare our method with other state-of-the-art detection methods on the  
 435 backbone of VGG16. The mAP of baseline for the large, medium and small scale  
 436 occlusion are 36.9%, 53.5% and 59.3%, which increase significantly after introducing  
 437 the OSGM and the OSIM further. For our GC-FRCN, the mAP of 50.5%, 61.1% and  
 438 65.1% for three occlusion scales, outperforming baseline by 13.6%, 7.6% and 5.8%.

439 Furthermore, among the purely one-stage detectors such as YOLO, YOLO V3 and  
440 SSD or the two-stage like A-FRCN (Wang et al., 2017), the best result of YOLO V3 is  
441 47.3% for large occlusion scale while 63.6% for small occlusion scale, which are  
442 lower by 3.2% and 1.5% than the GC-FRCN. The comparison results on the PASCAL  
443 VOC 2007 are presented in Table 1. The results show that GC-FRCN can effectively  
444 improve the detection accuracy of objects with different occlusion scales.

### 445 5.3.2 Ablative Analysis

446 **Hyper-parameter Analysis.** The  $\gamma_1$  and  $\gamma_2$  in formula (7) determine the  
447 influence of the generator and discriminators on the occlusion inpainting task, which  
448 is the key hyper-parameters in our OSIM. To find their optimal values, we conduct  
449 experiments using the OSIM model training from different  $\gamma_1$  and  $\gamma_2$ . We always set  
450 same value for  $\gamma_1$  and  $\gamma_2$ . Intuitively, it may make more sense to find out the  
451 relationship between our generator and discriminators due to the two discriminators  
452 working as a whole participate in the zero-sum game with the generator. As shown in  
453 Fig. 6, the detection performance (reported by mAP of big occlusion scale) can be  
454 obviously improved by setting the  $\gamma_1 = \gamma_2 = 300$ . We suppose the too small weight  
455 is difficult to contribute the key feature generation, and too large weight means too  
456 harsh on the generator and may result in a local optimal solution.



Different  $\gamma_1$  and  $\gamma_2$  for OSIM model

Fig. 6 The selection weights for local and global discriminator loss

457 **OSGM Analysis.** As shown in Table 2, to verify the effectiveness of OSGM, we  
 458 also compared it with other occlusion generation strategies. We used the occlusion  
 459 simulation strategy of discarding pixel values randomly on the original image as the  
 460 benchmark. At this time, take the small scale occlusion as an example, the mAP as  
 461 well as mAR of objects are 65.5% and 78.9%, and the model training time is about  
 462 610 minutes. The second strategy is to randomly discard pixels on the feature, whose  
 463 result shows that discarding pixels from the feature map is equivalent to discarding  
 464 original pixel values directly. When it comes to our OSGM which selects and discard  
 465 high-semantic feature points, the mAP and mAR only decreases by 0.3% and 0.5%  
 466 compared with the second strategy. We also find the training time has a dramatic  
 467 reduction in our OSGM, which decreases by nearly 33% in contrast to the second  
 468 strategy and decreases by more than 50% from baseline. We suppose that our OSGM  
 469 can significantly reduce the training cost during screen and produce high  
 470 representative and effective occlusion scenes.

471



472

Table 2 Results of GC-FRCN for **VOC 2007 test** with different OSIM drop strategies

Methods	mAP of different occlusion			mAR of different occlusion			Training time
	Big	Middle	Small	Big	Middle	Small	
Drop on image	50.6%	61.4%	65.5%	61.7%	73.1%	78.9%	610min
Drop on feature map	50.6%	61.3%	65.4%	61.7%	72.8%	78.7%	415min
Drop on Effective RF (OSGM)	50.5%	61.1%	65.1%	62.2%	72.5%	78.4%	275min

473

**OSIM Analysis.** We also use different loss function to train repair models and then

474

compare the detection accuracy of GC-FRCN for occlusion at different scales. The

475

simplest baseline method is to train the repair model using only the generation loss

476

$L_G$ , as shown in the first row of Table 3, whose mAP and mAR for the object with

477

small scale occlusion is 62.6% and 75.7%. In another set of experiments, we add local

478

discrimination loss  $L_{localD}$  to train the feature repair model, at which time the mAP

479

and mAR for small-scale occluded object increases by 1.4% and 0.8%. When the loss

480

function  $L_3$  is used to normalize the feature repair model, we show the optimized

481

occluded object which output by the global discriminator in Fig. 7. The visualization

482

results show that the OSIM structure in this paper can effectively remove the

483

occlusion noise in the feature. We obtain a mAP of 65.1% for the small-scale

484

occluded object, which increases by 2.5% and 1.1% in contrast to  $L_1$  and  $L_2$

485

respectively. Similarly, for the object with large or medium scale occlusion, the

486

detection accuracy of GC-FRCN still increases with the refinement of the repair

487

network structure and loss function. All the experimental results show that our OSIM

488

can improve the repair accuracy of the features and further improve the detection

489

accuracy of GC-FRCN.

490

491

Table 3 Results of GC-FRCN for **VOC 2007 test** with different OSIM loss functions

Different loss	Mechanism			mAP of different occlusion			mAR of different occlusion		
	$+L_G$	$+L_{localD}$	$+L_{globalD}$	Big	Middle	Small	Big	Middle	Small
$L_1$	✓			42.4%	56.5%	62.6%	54.9%	69.1%	75.7%
$L_2$	✓	✓		44.8%	57.8%	64.0%	57.3%	69.8%	76.5%
$L_3$	✓	✓	✓	50.5%	61.1%	65.1%	61.6%	72.7%	76.5%

493

In addition to the mAP of the detection, we also perform a quantitative evaluation

494

using the three loss functions on the three different occlusion scales. The results are

495

shown in Table 4. For the first row, we can see the SSIM is 0.703 for the small

496

occlusion scale while only fall by 3.2% for the big occlusion. Comparing to the results

497

of the second and third row with the discriminators, the SSIM of  $L_1$  shows a better

498

stability with the change of occlusion. We suppose this is because the  $L_1$  favors more

499

on the distance in pixel values simply. In other words, the  $L_1$  performs poorly as it

500

hardly recovers the useful semantics to some extent, which can explain the lower

501

mAP in Table 3. After adding discriminators, OSIM with the  $L_3$  achieves a SSIM of

502

0.728 for the big occlusion, which increases by 10.4% compared to the SSIM of 0.804

503

for the small occlusion. At the same time, we also find all SSIM of our OSIM with the

504

$L_3$  are better than the  $L_1$  and  $L_2$ . These gaps between different occlusion scales and

505

different loss functions show the validity and rationality of our OSIM with two

506

discriminators.

507

Table 4 SSIM of OSIM for **VOC 2007 test** with different loss functions

Different loss	Mechanism			SSIM of different occlusion		
	$+L_G$	$+L_{localD}$	$+L_{globalD}$	Big	Middle	Small
$L_1$	✓			0.671	0.686	0.703
$L_2$	✓	✓		0.695	0.731	0.746
$L_3$	✓	✓	✓	0.728	0.773	0.804

508

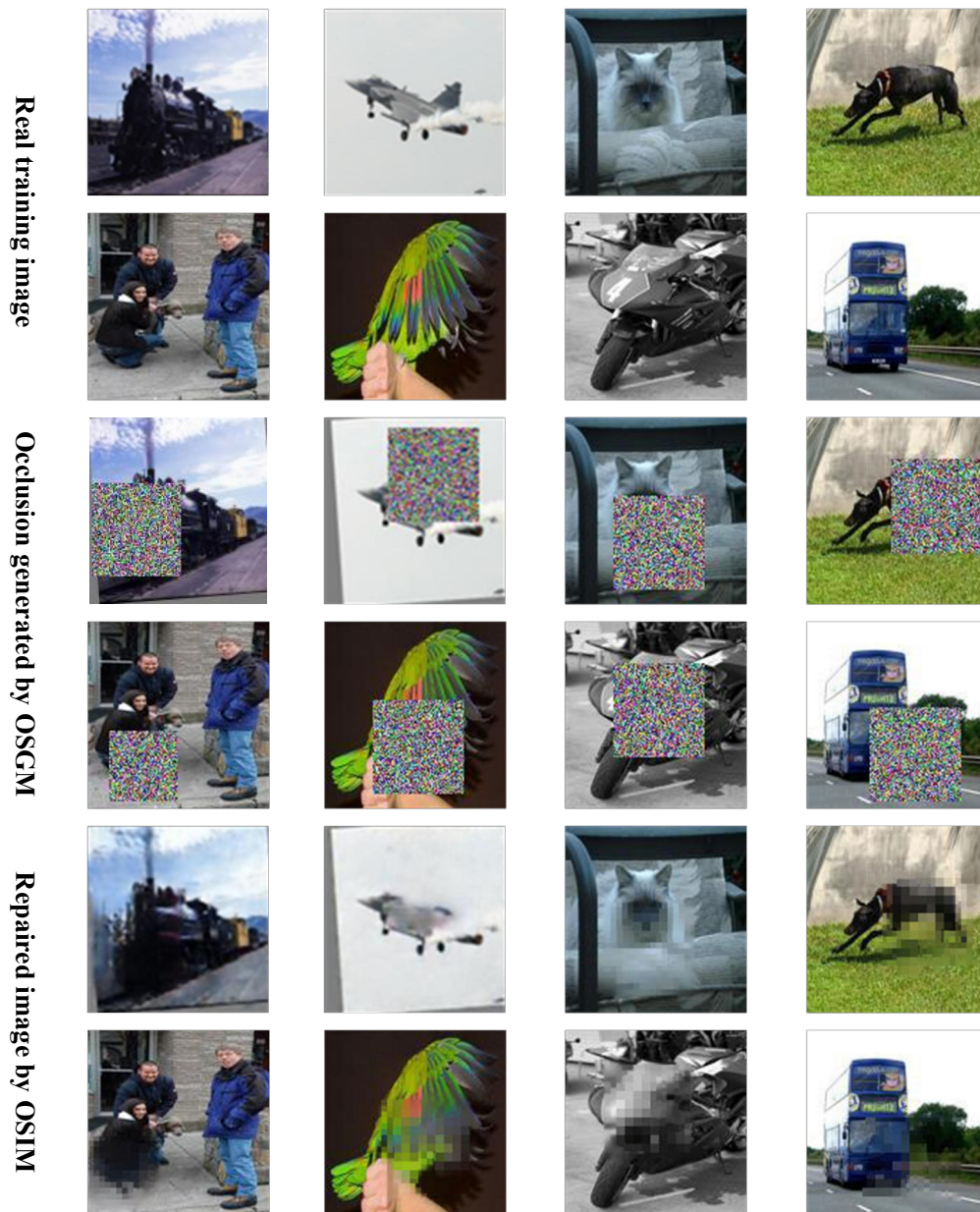


Fig. 7 Visual repair result based on OSIM

509 5.3.3 Category-based Analysis

510 Table 5 shows the change of detection accuracy of GC-FRCN and Faster RCNN for  
 511 different categories of objects under different scales of occlusions. Firstly, the  
 512 detection accuracy of GC-FRCN varies significantly for different kinds of objects.  
 513 Taking ‘bicycle’ and ‘train’ as examples, the AP of the three kinds of occlusion scales  
 514 are all over 59%, which can reach 76.5% and 74.6% respectively for the small-scale  
 515 occlusion. However, for ‘bottle’ and ‘potted plant’ with small scale occlusion, the APs

516 are only 40.1% and 34.9% respectively and will continue to decrease with the  
517 increase of occlusion scale. Moreover, we also find though our GC-FRCN can  
518 effectively improve the detection accuracy of most categories under different  
519 occlusion scales, the improvement of GC-FRCN is not obvious for some categories  
520 and even decrease slightly compared with the baseline method in some cases. More  
521 interestingly, these cases also mainly focus on the ‘bottle’ and ‘pottedplant’. The  
522 possible explanation is that compared with other objects, it is more difficult to learn  
523 features of small-size objects such as the ‘bottle’ and ‘potted plant’, which also makes  
524 it more difficult to deduce occlusion when using original real features.

525 Table 5 Changes of average precision of GC-FRCN relative to baseline for **VOC 2007 test**

Category	AP of GC-FRCN			AP of Faster-RCNN			Change of AP		
	Big	Middle	Small	Big	Middle	Small	Big	Middle	Small
aeroplane	49.3%	58.0%	66.6%	23.4%	42.4%	48.5%	26.0%	15.6%	18.1%
bicycle	63.1%	75.1%	76.5%	46.0%	69.0%	78.0%	17.1%	6.1%	-1.6%
bird	36.6%	54.1%	61.8%	30.3%	50.7%	53.5%	6.3%	3.4%	8.3%
boat	40.7%	47.7%	53.2%	27.3%	42.6%	43.4%	13.4%	5.1%	9.8%
bottle	31.1%	38.2%	40.1%	30.2%	41.8%	42.5%	0.9%	-3.6%	-2.4%
bus	63.0%	73.7%	72.3%	41.8%	61.8%	68.1%	21.3%	11.9%	4.2%
car	65.8%	74.2%	75.7%	52.7%	68.4%	75.1%	13.1%	5.8%	0.6%
cat	63.6%	74.4%	77.3%	40.8%	61.8%	69.0%	22.8%	12.6%	8.3%
chair	33.9%	43.7%	46.6%	22.3%	40.3%	42.9%	11.7%	3.4%	3.7%
cow	43.8%	62.5%	66.5%	38.7%	54.4%	61.8%	5.1%	8.1%	4.7%
diningtable	57.3%	67.2%	66.0%	42.2%	62.7%	61.6%	15.1%	4.6%	4.4%
dog	58.1%	70.7%	73.6%	37.4%	56.3%	64.9%	20.7%	14.3%	8.7%
horse	65.1%	73.7%	77.7%	52.2%	68.7%	75.4%	12.8%	4.9%	2.3%
motorbike	62.0%	69.9%	72.8%	43.2%	64.1%	66.4%	18.8%	5.7%	6.4%
person	54.9%	63.9%	68.5%	45.4%	56.7%	66.7%	9.5%	7.2%	1.8%
pottedplant	28.5%	32.9%	34.9%	28.8%	30.9%	35.4%	-0.3%	2.0%	-0.5%
sheep	33.9%	54.8%	64.6%	30.7%	51.1%	57.0%	3.1%	3.8%	7.6%
sofa	52.1%	61.7%	63.7%	33.2%	54.5%	58.6%	18.9%	7.1%	5.1%
train	59.0%	67.3%	74.6%	35.8%	49.6%	59.7%	23.2%	17.8%	14.9%
tvmonitor	49.1%	58.6%	68.5%	34.3%	42.5%	57.8%	14.8%	16.1%	10.8%

#### 526 5.3.4 Different Size of Occlusion Analysis

527 According to the results in table 1, for objects with large, medium and small scale

528 occlusion, the mAP of baseline is 36.9%, 53.5% and 59.3% respectively, which  
529 increase with the decrease of the occlusion scale. Other experimental results in table 1  
530 also verify this trend of accuracy change. For GC-FRCN, the mAP of objects in small  
531 scale occlusion is 65.1%, which is significantly increased by about 15% than that of  
532 objects in large scale occlusion. The change of occlusion scale directly describes the  
533 amount of occlusion noise and the loss degree of the original information. The above  
534 experimental results support the hypothesis that occlusion noise will directly affect  
535 the classification accuracy in this paper.

536 Secondly, for the OSGM and OSIM modules involved in GC-FRCN, we find that  
537 there are significant differences in the improvement of the accuracy of objects with  
538 different occlusion scales. Compared with the baseline, for the objects with three  
539 different occlusion scale, the detection accuracy increases by 2.2%, 1.6% and 7%  
540 after adding the OSGM module, while increases by 4.2%, 4.7% and 11.2% after  
541 adding the OSIM module respectively. The above experimental results show that  
542 compared with OSGM module based on data enhancement strategy, OSIM based on  
543 high-quality feature expression strategy has a more noticeable improvement in the  
544 detection accuracy of occluded objects. Besides, the improvement of detection  
545 accuracy of OSIM is more and more evident with the increase of occlusion scales.  
546 When analyzing this phenomenon in-depth, the reason may be the lack of available  
547 original effective information for the repairing of objects with large scale occlusion,  
548 which increases the difficulty of repairing and reduces the detection accuracy; In  
549 contrast, compared with the small scale occlusion object which retains most of the

550 real information, the rough feature optimization can significantly improve the feature  
551 quality and thus greatly improve the detection accuracy.

#### 552 5.4 Results on PASCAL VOC 2012 and MS COCO

553 We also verified the performance of GC-FRCN on PASCAL VOC 2012 data set  
554 and MS COCO data set. Taking small-scale occluded objects as an example, for VOC  
555 2012 data set, the mAP of Faster RCNN based on VGG-16 network is 64.8%, which  
556 reaches 69.4% by combining OSGM and OSIM, increasing by 4.6% than the baseline.  
557 Similarly, for the COCO data set, the mAP and mAR of baseline is only 21.7% and  
558 33.1%, which reaches 24.9% and 36.5% by combining OSGM and OSIM.

#### 559 5.5 Results on PANICLE2017

560 In order to verify the actual detection effect of GC-FRCN on occluded objects,  
561 we also applied it to the task of counting rice panicles in the field of current  
562 agricultural research. Getting the number of panicles automatic is the key to high  
563 throughput rice breeding and intelligent yield measurement, while it is a challenge as  
564 the panicle usually locally covered by leaves. The detection effect on rice panicles is  
565 shown in Fig. 8a, and LMM (Fernandez et al., 2018), Panicle-SEG (Xiong et al., 2017)  
566 and Faster-RCNN are selected as comparison objects. The average counting accuracy  
567 and classification accuracy of the four methods are shown in Table 6.

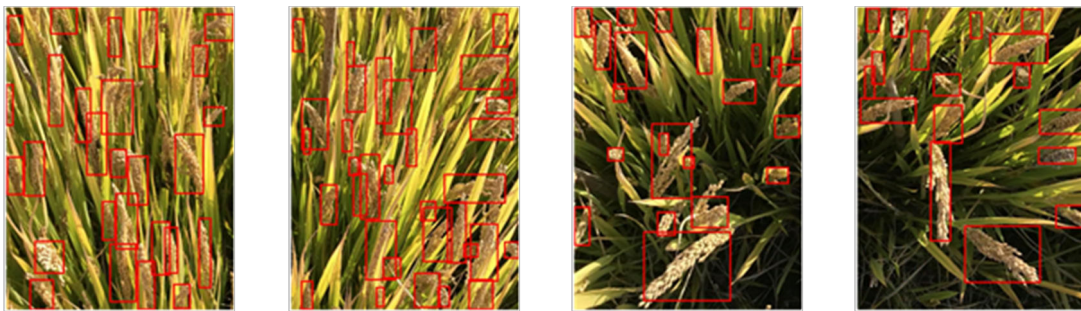
568 The average counting accuracy and classification accuracy of GC-FRCN are  
569 90.82% and 99.05% respectively, which are 16.12% and 5.15% higher than Faster  
570 RCNN algorithm, and about 8% and 4% higher than the similar counting algorithm.  
571 As shown in Fig. 8b, we analyze the detection effect of GC-FRCN on blocked rice

572 panicles further in detail. The green box in the visualization results represents the real  
 573 blocked rice panicles in the image, while the red box represents the detected results by  
 574 GC-FRCN. The above experimental results firstly verify the hypothesis that occlusion  
 575 noise will suppress the classification accuracy of object detection. Secondly, it also  
 576 shows that GC-FRCN can be applied to the detection and counting of rice panicles  
 577 partially blocked by leaves in complex field scenes by improving the feature quality.

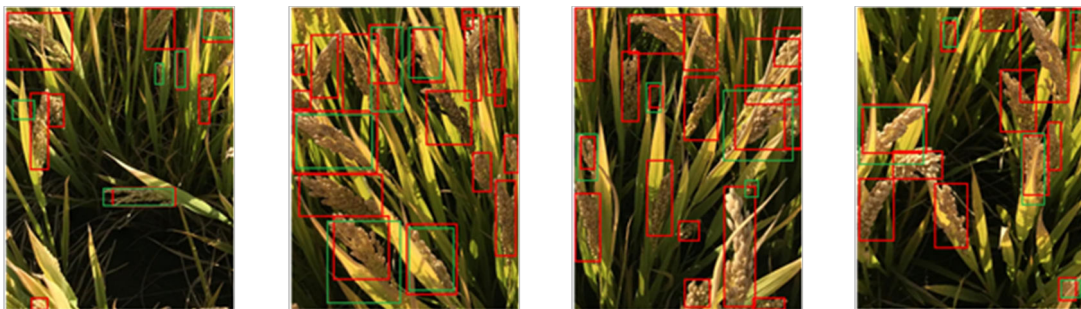
578 Table 6 Performance comparison of GC-FRCN and other approaches on PANICLE2017 test

Methods	Arch	$P_c$	$P_t$
		Average $\pm$ STD	Average $\pm$ STD
Faster-RCNN	VGG-16	74.12% $\pm$ 0.19%	93.85% $\pm$ 0.31%
LMM	/	82.16% $\pm$ 0.68%	95.18% $\pm$ 0.36%
Pan-seg	/	82.73% $\pm$ 0.91%	95.45% $\pm$ 0.62%
GC-FRCN (our)	VGG-16	90.82% $\pm$ 0.39%	99.05% $\pm$ 0.20%

579



(a) Detect effect of GC-FRCN for in-field rice panicle images



(b) Detect effect of GC-FRCN for panicles occluded by leaves locally

Fig8 Detect effect of GC-FRCN for PANICLE2017 test data set

## 580 6 Conclusion

581 In this paper, we propose a detection algorithm for occluded objects based on

582 generative feature optimization, for the problem of low feature quality rising from the  
583 external occlusion. Firstly, a quick and low-cost occlusion sample generation module  
584 OSGM is introduced, which realized the occlusion simulation and the enhancement of  
585 the original training data by screening and discarding the high semantic pixels on the  
586 feature map; Secondly, a feature repair module OSIM is introduced, which can repair  
587 the occlusion noise as the object's real feature to improve the feature quality. The  
588 results of ablation experiments verified the effectiveness of OSGM and OSIM. For  
589 the three standard data sets of VOC2007, VOC2012 and COCO, the results show that  
590 GC-FRCN can significantly improve the detection accuracy for objects with different  
591 scale occlusion. The results of PANICLE2017 data set also show that GC-FRCN can  
592 be applied to solve the practical problem of counting rice panicles partially occluded  
593 by leaves.

## 594 Acknowledge

595 This paper is supported in part by the National Natural Science Foundation of China  
596 (No. 31872847); and the Key Research and Development Plan of Jiangsu Province of  
597 China (Modern Agriculture, BE2019383).

## 598 Reference

- 599 [1]Ren S, He K, Girshick R, et al. Faster r-cnn: Towards real-time object detection with region  
600 proposal networks[C]//Advances in neural information processing systems. 2015: 91-99.
- 601 [2]He K, Gkioxari G, Dollár P, et al. Mask r-cnn[C]//Proceedings of the IEEE international  
602 conference on computer vision. 2017: 2961-2969.



603 [3]Cai Z, Fan Q, Feris R S, et al. A unified multi-scale deep convolutional neural network for fast  
604 object detection[C]//European conference on computer vision. Springer, Cham, 2016: 354-370.

605 [4]Law H, Deng J. Cornernet: Detecting objects as paired keypoints[C]//Proceedings of the  
606 European Conference on Computer Vision (ECCV). 2018: 734-750.

607 [5]Lu X, Li B, Yue Y, et al. Grid r-cnn[C]//Proceedings of the IEEE Conference on Computer  
608 Vision and Pattern Recognition. 2019: 7363-7372.

609 [6]Zhou X, Zhuo J, Krahenbuhl P. Bottom-up object detection by grouping extreme and center  
610 points[C]//Proceedings of the IEEE Conference on Computer Vision and Pattern Recognition.  
611 2019: 850-859.

612 [7]Duan K, Bai S, Xie L, et al. Centernet: Keypoint triplets for object detection[C]//Proceedings of  
613 the IEEE International Conference on Computer Vision. 2019: 6569-6578.

614 [8]Ouyang W, Zeng X, Wang X. Single-pedestrian detection aided by two-pedestrian detection[J].  
615 IEEE transactions on pattern analysis and machine intelligence, 2014, 37(9): 1875-1889.

616 [9]Tian Y, Luo P, Wang X, et al. Deep learning strong parts for pedestrian  
617 detection[C]//Proceedings of the IEEE international conference on computer vision. 2015:  
618 1904-1912.

619 [10]Wang X, Xiao T, Jiang Y, et al. Repulsion loss: Detecting pedestrians in a  
620 crowd[C]//Proceedings of the IEEE Conference on Computer Vision and Pattern Recognition.  
621 2018: 7774-7783.

622 [11]Zhang S, Wen L, Bian X, et al. Occlusion-aware R-CNN: detecting pedestrians in a  
623 crowd[C]//Proceedings of the European Conference on Computer Vision (ECCV). 2018: 637-653.

624 [12]Bell S, Lawrence Zitnick C, Bala K, et al. Inside-outside net: Detecting objects in context with

625 skip pooling and recurrent neural networks[C]//Proceedings of the IEEE conference on computer  
626 vision and pattern recognition. 2016: 2874-2883.

627 [13]Lin T Y, Dollár P, Girshick R, et al. Feature pyramid networks for object  
628 detection[C]//Proceedings of the IEEE conference on computer vision and pattern recognition.  
629 2017: 2117-2125.

630 [14]Pepikj B, Stark M, Gehler P, et al. Occlusion patterns for object class  
631 detection[C]//Proceedings of the IEEE Conference on Computer Vision and Pattern Recognition.  
632 2013: 3286-3293.

633 [15]Mathias M, Benenson R, Timofte R, et al. Handling occlusions with  
634 franken-classifiers[C]//Proceedings of the IEEE International Conference on Computer Vision.  
635 2013: 1505-1512.

636 [16]Tang S, Andriluka M, Schiele B. Detection and tracking of occluded people[J]. International  
637 Journal of Computer Vision, 2014, 110(1): 58-69.

638 [17]Gidaris S, Komodakis N. Object detection via a multi-region and semantic  
639 segmentation-aware cnn model[C]//Proceedings of the IEEE international conference on computer  
640 vision. 2015: 1134-1142.

641 [18]Zhou C, Yuan J. Multi-label learning of part detectors for heavily occluded pedestrian  
642 detection[C]//Proceedings of the IEEE International Conference on Computer Vision. 2017:  
643 3486-3495.

644 [19]Noh J, Lee S, Kim B, et al. Improving occlusion and hard negative handling for single-stage  
645 pedestrian detectors[C]//Proceedings of the IEEE Conference on Computer Vision and Pattern  
646 Recognition. 2018: 966-974.

647 [20]Papageorgiou C, Poggio T. A trainable system for object detection[J]. International journal of  
648 computer vision, 2000, 38(1): 15-33.

649 Viola P, Jones M J. Robust real-time face detection[J]. International journal of computer vision,  
650 2004, 57(2): 137-154.

651 [21]Felzenszwalb P, McAllester D, Ramanan D. A discriminatively trained, multiscale,  
652 deformable part model[C]//2008 IEEE Conference on Computer Vision and Pattern Recognition.  
653 IEEE, 2008: 1-8.

654 [22]Felzenszwalb P F, Girshick R B, McAllester D, et al. Object detection with discriminatively  
655 trained part-based models[J]. IEEE transactions on pattern analysis and machine intelligence,  
656 2009, 32(9): 1627-1645.

657 [23]Dollár P, Appel R, Belongie S, et al. Fast feature pyramids for object detection[J]. IEEE  
658 transactions on pattern analysis and machine intelligence, 2014, 36(8): 1532-1545.

659 [24]Girshick R, Donahue J, Darrell T, et al. Rich feature hierarchies for accurate object detection  
660 and semantic segmentation[C]//Proceedings of the IEEE conference on computer vision and  
661 pattern recognition. 2014: 580-587.

662 [25]Uijlings J R R, Van De Sande K E A, Gevers T, et al. Selective search for object recognition[J].  
663 International journal of computer vision, 2013, 104(2): 154-171.

664 [26]He K, Zhang X, Ren S, et al. Spatial pyramid pooling in deep convolutional networks for  
665 visual recognition[J]. IEEE transactions on pattern analysis and machine intelligence, 2015, 37(9):  
666 1904-1916.

667 [27]Girshick R. Fast r-cnn[C]//Proceedings of the IEEE international conference on computer  
668 vision. 2015: 1440-1448.

669 [28]Ren S, He K, Girshick R, et al. Faster r-cnn: Towards real-time object detection with region  
670 proposal networks[C]//Advances in neural information processing systems. 2015: 91-99.

671 [29]Dai J, Li Y, He K, et al. R-fcn: Object detection via region-based fully convolutional  
672 networks[C]//Advances in neural information processing systems. 2016: 379-387.

673 [30]Redmon J, Divvala S, Girshick R, et al. You only look once: Unified, real-time object  
674 detection[C]//Proceedings of the IEEE conference on computer vision and pattern recognition.  
675 2016: 779-788.

676 [31]Liu W, Anguelov D, Erhan D, et al. Ssd: Single shot multibox detector[C]//European  
677 conference on computer vision. Springer, Cham, 2016: 21-37.

678 [32]Redmon J, Farhadi A. YOLO9000: better, faster, stronger[C]//Proceedings of the IEEE  
679 conference on computer vision and pattern recognition. 2017: 7263-7271.

680 [33]Redmon J, Farhadi A. Yolov3: An incremental improvement[J]. arXiv preprint  
681 arXiv:1804.02767, 2018.

682 [34]Simo-Serra E, Trulls E, Ferraz L, et al. Fracking deep convolutional image descriptors[J].  
683 arXiv preprint arXiv:1412.6537, 2014.

684 [35]Loshchilov I, Hutter F. Online batch selection for faster training of neural networks[J]. arXiv  
685 preprint arXiv:1511.06343, 2015.

686 [36]Wang X, Gupta A. Unsupervised learning of visual representations using  
687 videos[C]//Proceedings of the IEEE International Conference on Computer Vision. 2015:  
688 2794-2802.

689 [37]Shrivastava A, Gupta A, Girshick R. Training region-based object detectors with online hard  
690 example mining[C]//Proceedings of the IEEE conference on computer vision and pattern

691 recognition. 2016: 761-769.

692 [38]Wang X, Shrivastava A, Gupta A. A-fast-rcnn: Hard positive generation via adversary for  
693 object detection[C]//Proceedings of the IEEE Conference on Computer Vision and Pattern  
694 Recognition. 2017: 2606-2615.

695 [39]Xiang P, Wang L, Cheng J, et al. A deep network architecture for image inpainting[C]//2017  
696 3rd IEEE International Conference on Computer and Communications (ICCC). IEEE, 2017:  
697 1851-1856.

698 [40]Lahiri A, Jain A, Biswas P K, et al. Improving Consistency and Correctness of Sequence  
699 Inpainting using Semantically Guided Generative Adversarial Network[J]. arXiv preprint  
700 arXiv:1711.06106, 2017.

701 [41]Yeh R A, Chen C, Yian Lim T, et al. Semantic image inpainting with deep generative  
702 models[C]//Proceedings of the IEEE Conference on Computer Vision and Pattern Recognition.  
703 2017: 5485-5493.

704 [42]Dolhansky B, Canton Ferrer C. Eye in-painting with exemplar generative adversarial  
705 networks[C]//Proceedings of the IEEE conference on computer vision and pattern recognition.  
706 2018: 7902-7911.

707 [43]Pathak D, Krahenbuhl P, Donahue J, et al. Context encoders: Feature learning by  
708 inpainting[C]//Proceedings of the IEEE conference on computer vision and pattern recognition.  
709 2016: 2536-2544.

710 [44]Li Y, Liu S, Yang J, et al. Generative face completion[C]//Proceedings of the IEEE  
711 Conference on Computer Vision and Pattern Recognition. 2017: 3911-3919.

712 [45]Yu J, Lin Z, Yang J, et al. Generative image inpainting with contextual

713 attention[C]//Proceedings of the IEEE Conference on Computer Vision and Pattern Recognition.  
714 2018: 5505-5514.

715 [46]Luo W, Li Y, Urtasun R, et al. Understanding the effective receptive field in deep  
716 convolutional neural networks[C]//Advances in neural information processing systems. 2016:  
717 4898-4906.

718 [47]Simonyan K, Zisserman A. Very deep convolutional networks for large-scale image  
719 recognition[J]. arXiv preprint arXiv:1409.1556, 2014.

720 [48]Everingham M, Van Gool L, Williams C K I, et al. The pascal visual object classes (voc)  
721 challenge[J]. International journal of computer vision, 2010, 88(2): 303-338.

722 [49]Lin T Y, Maire M, Belongie S, et al. Microsoft coco: Common objects in  
723 context[C]//European conference on computer vision. Springer, Cham, 2014: 740-755.

724 [50]Fernandez-Gallego J A, Kefauver S C, Gutiérrez N A, et al. Wheat ear counting in-field  
725 conditions: high throughput and low-cost approach using RGB images[J]. Plant methods, 2018,  
726 14(1): 22-34.

727 [51]Xiong X, Duan L, Liu L, et al. Panicle-SEG: a robust image segmentation method for rice  
728 panicles in the field based on deep learning and superpixel optimization[J]. Plant methods, 2017,  
729 13(1): 104-119.